

Nanoscale

Accepted Manuscript

This article can be cited before page numbers have been issued, to do this please use: H. Lee, J. A. Muñoz-Castañeda and H. Ren, *Nanoscale*, 2025, DOI: 10.1039/D4NR04564E.



This is an Accepted Manuscript, which has been through the Royal Society of Chemistry peer review process and has been accepted for publication.

Accepted Manuscripts are published online shortly after acceptance, before technical editing, formatting and proof reading. Using this free service, authors can make their results available to the community, in citable form, before we publish the edited article. We will replace this Accepted Manuscript with the edited and formatted Advance Article as soon as it is available.

You can find more information about Accepted Manuscripts in the [Information for Authors](#).

Please note that technical editing may introduce minor changes to the text and/or graphics, which may alter content. The journal's standard [Terms & Conditions](#) and the [Ethical guidelines](#) still apply. In no event shall the Royal Society of Chemistry be held responsible for any errors or omissions in this Accepted Manuscript or any consequences arising from the use of any information it contains.

Facet-Controlled Electrosynthesis of Nanoparticles by Combinatorial Screening in Scanning Electrochemical Cell Microscopy

Heekwon Lee^{1,†}, Jesús Alberto Muñoz-Castañeda^{1,†}, Hang Ren^{1, 2, 3,*}

1. Department of Chemistry, University of Texas at Austin, Austin, Texas 78712, United States

2. Texas Materials Institute, University of Texas at Austin, Austin, Texas 78712, United States

3. Allen J. Bard Center for Electrochemistry, University of Texas at Austin, Austin, Texas 78712, United States

[†]Authors contributed equally

*Corresponding author: hren@utexas.edu

ABSTRACT

Controlled synthesis of faceted nanoparticles on the surface without explicit use of ligands has gained attention due to their potential applications in electrocatalysis and sensing. Electrodeposition is a desirable method, but controlling the size, spatial distribution, and morphology of the nanoparticles requires extensive optimization. Here, we report spatially resolved synthesis of shape-controlled Pt nanoparticles and fast screening of synthesis conditions in scanning electrochemical cell microscopy (SECCM) using pulse potentials. Screening occurs at individual $\sim\mu\text{m}^2$ areas isolated in SECCM, allowing multiple conditions to be screened in one mapping experiment. The screening reveals that the formation of (100) facets in Pt nanoparticles is sensitive to the upper and lower potential limits in the square-wave potential pulse. The facet control is explained by the facet-dependent migration effect from the concurrent hydrogen evolution reaction during Pt deposition. Moreover, the density and size of nanoparticles can also be controlled. This approach paves the way for automated synthesis and characterization of single-facet metallic nanoparticles, offering great potential for advancements in electrocatalysis and sensor applications.

KEYWORDS: Electrodeposition; nanoparticles; single crystal; scanning electrochemical cell microscopy; platinum

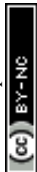


INTRODUCTION

Here, we report the facet-controlled electrosynthesis of nanoparticles directly on the electrode surface without added ligand by scanning electrochemical cell microscopy (SECCM). The use of SECCM enables fast screening of square-wave potentials used in the synthesis by varying the parameters within the same map in SECCM. The experimental results with colocalized characterization not only allow for the selective synthesis of cubic Pt nanoparticles with (100) facets but also help reveal an unconventional mechanism of differential local migration that leads to facet selectivity. The ability to control the facets in the nanoparticle in ligand-free electrodeposition directly on the substrate surface enables extra control in synthesizing nanoparticle libraries under SECCM, contributing to the high-throughput precision synthesis and screening of nanomaterials.

Metallic nanoparticles have physical and chemical properties that are applied to many applications, such as catalysis, optics, electronics, and biology.¹⁻³ The properties are intricately related to their size, shape, and composition, which can be finely tuned by precision synthesis processes. Faceted metallic nanoparticles have attracted considerable interest because of their well-defined surface structures, which offer a good model system to study structure-property relationships beyond single crystal substrates.^{4,5} These facet nanoparticles have also shown applications in catalysis.⁶⁻⁸

Various chemical methods, such as wet chemistry, have been developed for synthesizing facet-controlled nanoparticles.^{7,9-11} However, such approaches often involve the use of ligands that bind to the nanoparticle surface, which can obstruct the active sites for catalysis, and undermine the interpretation of the structure-activity relationship. Their removal requires additional purification steps, and the trace amount of ligand after purification, if any, is also challenging to characterize. Additionally, these particles need to be immobilized on a substrate electrode in the application of electrocatalysis and electrochemical sensors. In contrast, electrochemical synthesis of nanoparticles is an effective alternative method.¹²⁻¹⁴ In electrochemical synthesis, the driving force, i.e., the potential on the electrode, can be readily controlled in real-time, allowing for precise control of the nucleation and growth processes during synthesis. The rate of electrodeposition can be monitored as the current, enabling quantitative control over nanoparticle size. Moreover, these particles are directly synthesized on the substrate electrode surface, eliminating the extra step of immobilization.

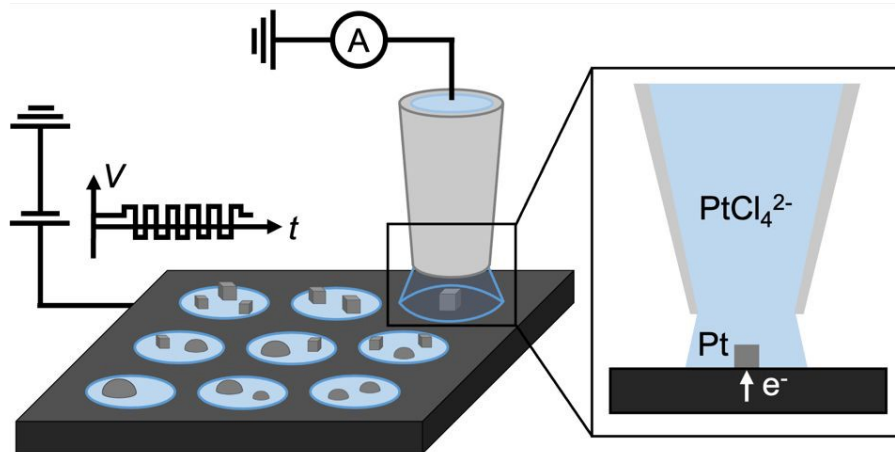


Advanced potential waveforms beyond DC potential, e.g., square waves have enabled the synthesis of nanoparticles with specific facet orientations without the addition of ligands.^{5,15–18} These nanoparticles have demonstrated superior catalytic performance, e.g., in ethanol oxidation and formic acid oxidation, which are highly sensitive to the facet.^{15,19} However, the throughput for optimizing the experimental conditions is low as one set of parameters requires one electrode. Scanning electrochemical cell microscopy (SECCM) is a powerful tool for the controlled electrodeposition of nanoparticles with spatial resolution.^{20,21} The movement of droplet cells in SECCM allows thousands of electrochemical experiments performed on the same substrate, which can significantly increase the throughput of the electrochemical experiments.^{22–24} For example, Although the SECCM configuration has a limitation in the quantity of nanoparticle synthesis produced at the same time compared to wet chemistry, SECCM has been successfully employed in the deposition of silver nanoparticles, both as single deposits and as arrays, as well as in the synthesis of bimetallic nanoparticles with controlled composition.^{25–27}

Herein, we use SECCM coupled with potential pulses to screen facet-controlled metallic nanoparticles in a combinatorial manner. Multiple conditions of the square-wave potentials, including the upper/lower potentials, and the frequency, can be screened on the same substrate. Colocalized characterization with electron microscopy and atomic force microscopy demonstrates the conditions important to control the facet, size, and density of nanoparticles under SECCM. The approach offers additional fine control, especially the facet, in the synthesis of nanoparticle libraries in SECCM, which moves towards automated nanoparticle synthesis and accelerated materials discovery, especially suitable for discovering electrocatalysts.

RESULTS AND DISCUSSION





Scheme 1. Schematic illustration of shaped controlled electrodeposition of a metal nanoparticle array by SECCM.

A single-channel SECCM setup was employed for electrodeposition of shape-controlled Pt nanoparticles using square-wave potentials, as illustrated in **Scheme 1**. A single-barrel nanopipette with a typical opening radius of ~ 420 nm (**Figure S1**) was filled with Pt precursor solution (0.5 mM Na_2PtCl_4 + 100 mM H_2SO_4). The precise positioning of the nanopipette, as commonly practiced in SECCM to contact the meniscus at the pipette tip with the glassy carbon (GC) substrate, completes the circuit and triggers a sudden current flow. This current spike provides the feedback to temporarily park the nanopipette at the surface and initiate the square-wave pulses for Pt deposition (see the experimental setup details in **SI Section S1**). The contact area between the droplet and the substrate defines the localized electroactive area for electrodeposition. The upper and lower limit potentials (E_L and E_U), frequency (f), and duration (t_d) of square-wave potentials can modulate the morphology of the resulting nanoparticles. After completion of each deposition, the pipette is retracted and moved to a new location, where the electrodeposition condition can be varied. Details of each experimental sequence in SECCM are illustrated in **Scheme S2** in **SI Section S3**. Note that the substrate with nanoparticles was gently rinsed to eliminate residual Pt salts.



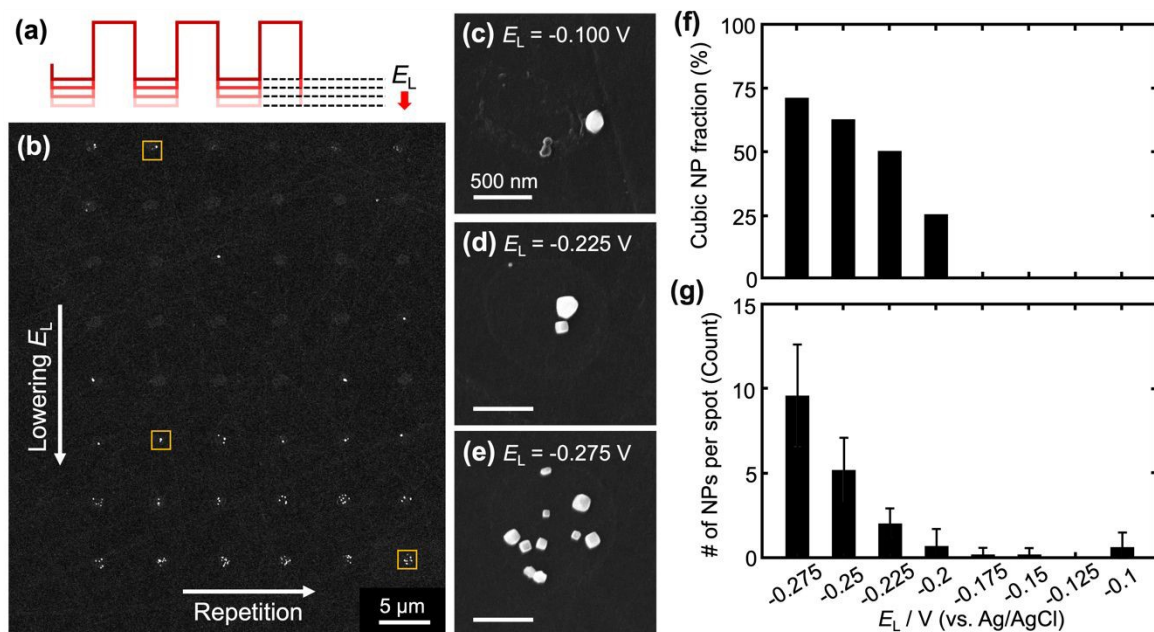


Figure 1. Electrosynthesis of Pt nanoparticle arrays with varying E_L in SECCM. (a) Schematic of the potential waveform. (b) SEM images of arrays of Pt nanoparticles synthesized. E_L varies from -0.1 to -0.275 V from top to bottom, with a step of 25 mV between the rows. Each condition is repeated 6 times along the row. (c-e) High-magnification SEM micrographs of individual deposition spots at various E_L . (f) Fraction of cubic nanoparticles as a function of E_L . (g) Number of nanoparticles per spot as a function of E_L . Electrolyte: 0.5 mM Na_2PtCl_4 + 100 mM H_2SO_4 . Deposition conditions: $E_U = 1.24$ V, $f = 500$ Hz, $t_d = 5$ s; E_L was varied.

The shape-controlled electrodeposition of Pt nanoparticles was systematically investigated by varying one of the parameters of the square wave at a time (i.e., E_L , E_U , f , and t_d). In the first set of experiments, E_L was varied while other parameters were kept constant ($E_U = 1.24$ V, $f = 500$ Hz, and $t_d = 5$ s). As the SEM images in **Figure 1** show, the morphology of the Pt nanoparticles is highly sensitive to E_L . At $E_L = -0.1$ V, the nanoparticles primarily exhibited rounded shapes on the substrate. A gradual transition in nanoparticle morphology was observed as E_L decreased. At E_L of -0.275 V, cubic nanoparticles were formed. The total number of nanoparticles per deposition spot also increased with decreasing E_L (**Figure 1g**). This is because more negative potentials promote nucleation, leading to a higher density of nanoparticles at each SECCM spot.

Atomic force microscopy (AFM) was employed to further characterize the morphology of the synthesized Pt nanoparticles deposited under two different E_L , and the topographic micrographs and line-scan profiles are shown in **Figure 2**. At a lower E_L (-0.275 V), nanoparticles show flat top planes (**Figures 2a-b**), consistent with the cubic morphology observed under SEM. The square planes on the cubic nanoparticles are (100) facets. In contrast, rounded nanoparticles



were obtained at higher E_L (-0.1 V) as shown in **Figures 2d-e**. The rounded-shaped profile suggests no preference for specific facets. Similar round shapes were also observed under constant-potential deposition (**Figure S3** and **SI Section S5**). The AFM analysis corroborates the SEM findings and highlights the sensitive dependence of facet formation on the lower potentials of the square wave used in electrodeposition.

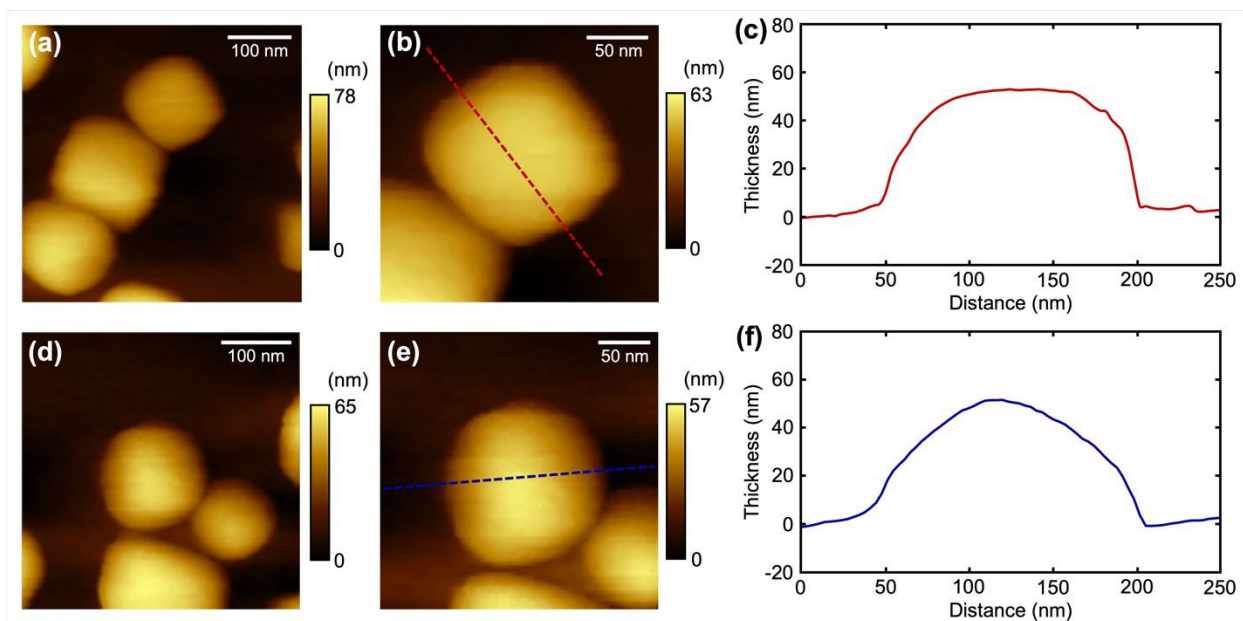
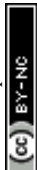


Figure 2. Atomic force microscopy of the electrosynthesized Pt nanoparticles. (a-b) Topographic images of cubic Pt nanoparticles and (c) the line profile. Deposition conditions: $E_L = -0.275$ V, $E_U = 1.24$ V, $f = 500$ Hz, and $t_d = 5$ s. (d-e) Topographic AFM images of rounded Pt nanoparticles and (f) the line profile. Deposition conditions: $E_L = -0.1$ V, rest conditions are the same as (a)-(c).

Next, we studied the effect of E_U in the square-wave potential on the morphology and density of Pt nanoparticles. E_U was varied from 1.04 to 1.34 V with an increment of 0.05 V, while other waveform parameters were kept the same ($E_L = -0.275$ V, $f = 500$ Hz, and $t_d = 5$ s). The results in **Figure S4** show that the total number of nanoparticles decreases as E_U increases. The half-cycle of E_U in the waveform is at the potential where Pt can be oxidized. Therefore, the decrease in particle number with increasing E_U is likely because some small Pt are anodically etched and dissolved. In addition, the fraction of cubic nanoparticles increases as a function of E_U (see **SI Section S6**).



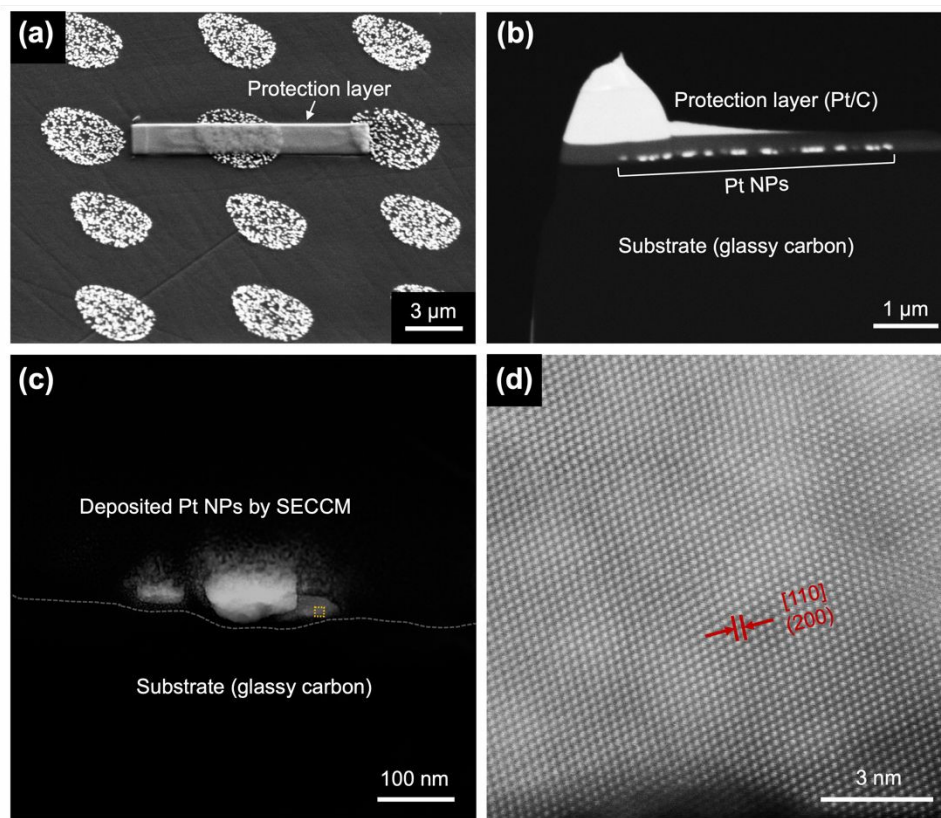


Figure 3. High-resolution scanning transmission electron microscopy (STEM) analysis of electrodeposited Pt nanoparticles prepared via SECCM. (a) SEM image of electrodeposited Pt nanoparticles with protective layers prior to focused ion beam (FIB) cutting (b) Overview SEM image of Pt nanoparticles deposited on a GC substrate with protective layers of C/Pt, and (c) a magnified view of electrodeposited nanoparticles on the substrate surface with a yellow dashed box highlighting (d) the atomic arrangement of Pt nanoparticles showing the (200) plane along the [110] zone axis.

To further analyze the atomic structures of the cubic Pt nanoparticles fabricated by SECCM, high-resolution scanning transmission electron microscopy (STEM) was employed to analyze the nanoparticles obtained using conditions that maximized the fraction of cubic morphology (i.e., $E_U = 1.24$, $E_L = -0.275$ V, $f = 500$ Hz, and $t_d = 5$ s) using a ~ 3 μm diameter pipette. **Figure 3a-c** shows the TEM lamella sample preparation to lift out the Pt nanoparticle deposited in SECCM to expose their cross sections. Detailed procedures of TEM specimen preparation are provided in SI **Section S7**. As depicted in **Figure 3d**, a low-index facet with (200) crystal orientation along the [110] zone axis is observed, which aligns with the final morphology of cubic Pt nanoparticles. A d-spacing of 1.96 \AA is attributed to the (200) plane in the FCC structure of Pt.



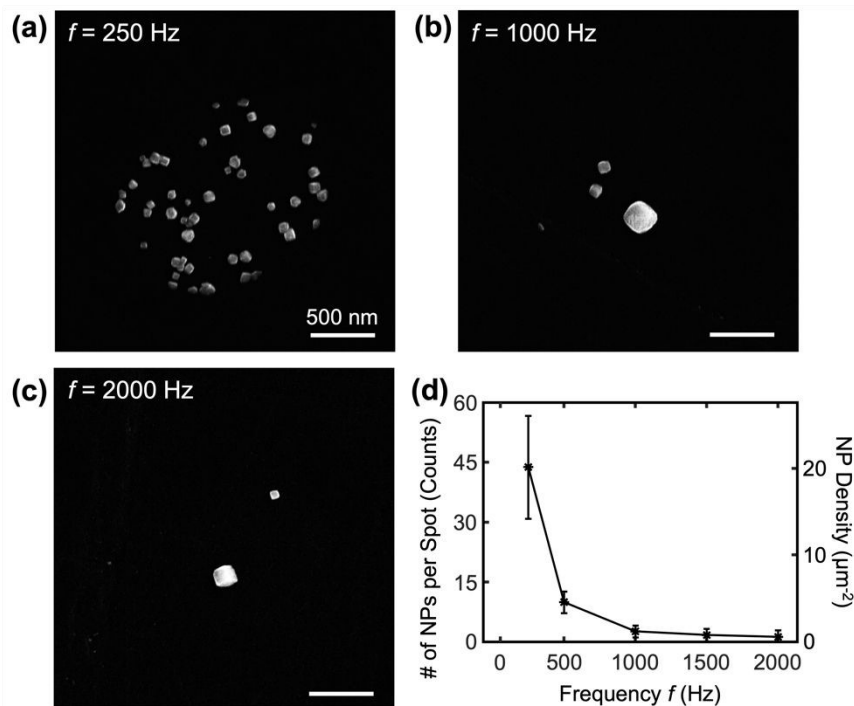


Figure 4. Frequency vs. number of Pt nanoparticles. (a-c) SEM images of nanocubes deposited at different f (a) 250, (b) 1000, and (c) 2000 Hz. (d) Number of nanoparticles per spot (left) and nanoparticle density (right) vs frequency of the square wave. Deposition conditions: $E_U = 1.24$ V, $E_L = -0.275$ V, and $t_d = 5$ s.

The effect of the frequency of the square-wave potential on the nanoparticle synthesis is further studied under SECCM in a similar fashion with increasing frequency in each row of the SECCM scan. **Figure 4** exhibits SEM images of nanocubes deposited at square-wave frequencies ranging from 250 to 2000 Hz, with other conditions unchanged ($E_U = 1.24$ V, $E_L = -0.275$ V, and t_d of 5 s). First, no significant dependence of the shape of the nanoparticle on the frequency was observed, but the density of nanoparticles was affected by the frequency. At the lowest frequency of 250 Hz (**Figure 4a**), the deposition results in ~ 44 nanocubes per spot (or $18 \mu\text{m}^{-2}$), indicating a high nucleation and growth rate. As the frequency was increased to 1000 Hz, the average number of nanoparticles decreased to 1.2 ($0.49 \mu\text{m}^{-2}$) in each spot, as shown in **Figure 4b**. When the frequency was increased to 2000 Hz, the individual deposition spots contained zero, one, or few nanoparticles (**Figure 4c**). The result suggests that higher frequencies of square waves decrease the nucleation rate. The relationship of decreasing density of nanoparticles with square-wave frequency is summarized in **Figure 4d**, and more electron micrographs are included in **Figure S6**.



The observation that higher particle density with decreasing square-wave potential is intriguing because the total time spent in the nucleation potential (i.e., the total time spent at E_U) in a given square wave is unchanged with frequency. The possible explanation is a two-step process where a pre-nucleation step needs to occur before the nucleation step, which warrants a separate detailed study. The tunable control over the density of nanoparticles via square-wave frequency highlights the versatility of SECCM in nanoparticle synthesis, allowing for the optimization of deposition conditions to achieve the designed nanoparticle density and morphology. Note that the upper limit of the frequency was estimated to be 4.2 kHz, which is confined by the RC time constant in the electrochemical system (see SI Section S9).

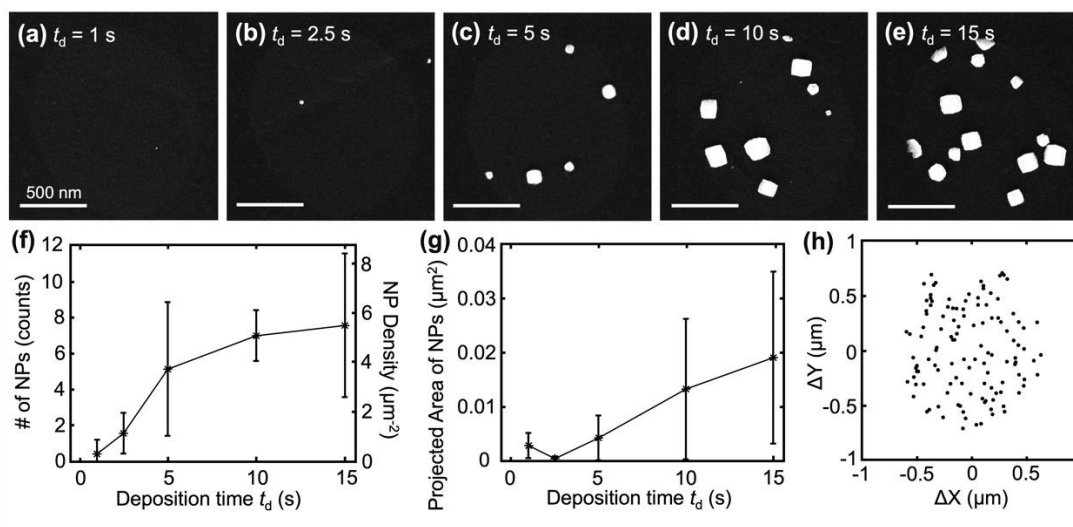


Figure 5. Size control of Pt nanocubes (a-e) SEM images of nanocubes electrodeposited with varying the deposition time t_d from 1 to 15 sec ($E_U = 1.24$ V, $E_L = -0.275$ V, and $f = 500$ Hz) (f-g) Relationships between (f) the number of synthesized particles and (g) the projected area of the deposited particles at different t_d from 0 to 15 sec. (h) Scatter plot showing particle offsets measured from total 120 Pt nanoparticles electrodeposited with varying t_d .

Lastly, we demonstrate that the size of nanoparticles can be controlled by the deposition time of the square wave, t_d . The effect of t_d on nanoparticle growth was systematically studied by varying t_d from 1 to 15 seconds while keeping the potential and frequency constant for cubic nanoparticle deposition ($E_U = 1.24$ V, $E_L = -0.275$ V, $f = 500$ Hz). SEM images of the nanoparticles synthesized at different t_d are shown in **Figures 5a-e**. At the shortest t_d of 1 s, only a few small nanoparticles were observed (**Figure 5a**), indicating limited nucleation and growth. As the t_d increased to 5 s (**Figure 5b**), the number and size of the nanoparticles increased, with more well-



defined nanocubes being formed. Further increasing t_d to 15 s resulted in a significant increase in both the number and size of the nanoparticles (**Figures 5c-e**). The increase in the number of nanoparticles with t_d is summarized in **Figure 5f**. This suggests that nucleation and growth continue to occur with time, similar to the process of progressive nucleation.²⁸ Additionally, the growth of the nanoparticles over time is further confirmed by the projected area of the deposited particles vs t_d , as shown in **Figure 5g**. Lastly, the spatial distribution of the nucleation sites from all deposition times is assessed by plotting the center of the Pt nanoparticle with respect to the center of the droplet. As shown in **Figure 5h**, a random distribution of nucleation sites is observed with no preferred location within the droplet in SECCM observed under square-wave potential modulation, suggesting the uniform accessibility of the entire electrode surface under the droplet under this condition. This random distribution suggests that the conclusions discovered here will likely apply to macroscale electrodes whenever the electrode is uniformly accessible. The statistical analysis of the spatial distribution of the nucleation sites is shown in SI **Section S10**.

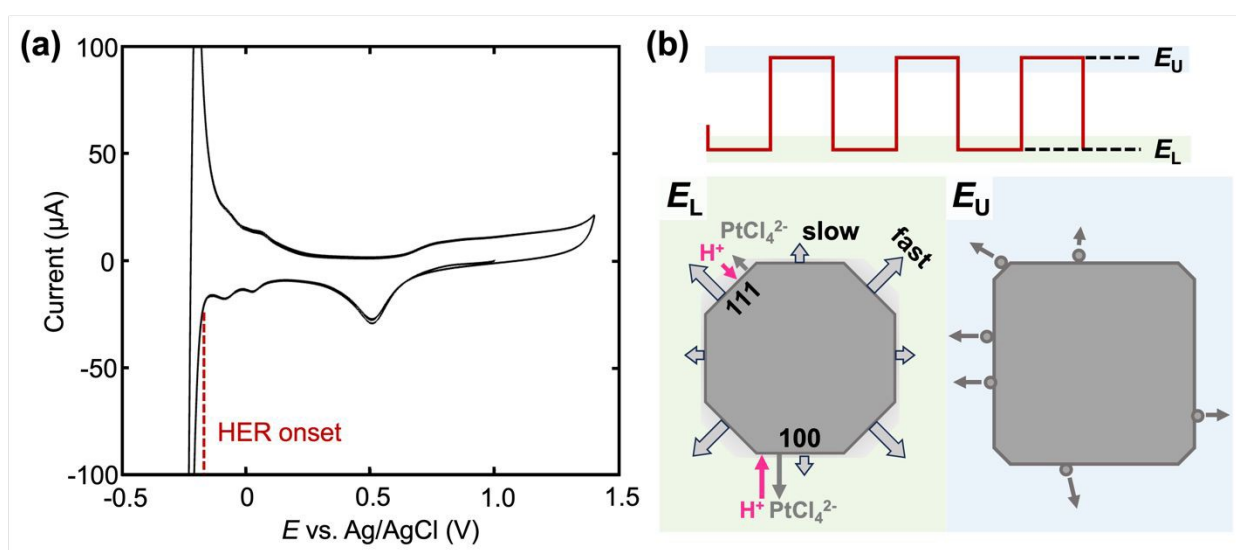


Figure 6. Proposed mechanism of Pt nanoparticles. (a) Cyclic voltammogram showing the onset of HER on Pt disk electrode (2 mm diameter). Three consecutive cycles are shown with an initial potential of 1 V. Solution: 100 mM H₂SO₄; reference electrode: Ag/AgCl; counter electrode: Pt wire; scan rate: 0.1 V/s. (b) Schematic illustration of square-wave potential waveform oscillating between upper (E_U) and lower (E_L) potentials.

The overall control that square-wave potential offers in the electrosynthesis of Pt nanoparticles can be understood as follows. The transition of a rounded-shaped particle to a cubic



one occurs when E_L is below -0.2 V (vs. Ag/AgCl), which overlaps with the onset of hydrogen evolution reaction (HER) on Pt as shown in the macroelectrode voltammogram in **Figure 6a**. This suggests that HER and Pt deposition from PtCl_4^{2-} occurs simultaneously when cubic nanoparticles are formed during the E_L half cycle of the square wave. The local HER current in acid is expected to be higher on Pt(100) compared to Pt(111) according to single-crystal electrochemical studies previously reported,²⁹ which induces more migration of PtCl_4^{2-} away from the surface. As illustrated in **Figure 6b**, the enhanced migration of PtCl_4^{2-} lowers the surface concentration of Pt precursor to a larger extent at (100) compared to (111), making Pt deposition slower on (100). The slower deposition on (100) compared to other facets preserves the (100) facet in the final nanoparticle. During the E_U half-cycle, Pt is anodically etched. The low-coordinated atoms are etched faster, leaving behind high-coordinated atoms, creating low-index facets on Pt nanoparticles.¹⁸ Moreover, the presence of SO_4^{2-} ions further aids this process by preferentially adsorbing onto the Pt (100) surface, stabilizing these facets and promoting the formation of cubic-like nanoparticles.^{30,31} Note that although the mass transfer is often the limiting step in acid HER on Pt instead of charge transfer, pulse-potential conditions significantly increase the mass transfer, explaining the importance of using square waves in controlling the facets.

CONCLUSIONS

In summary, a precision electrosynthesis method is developed for facet-controlled nanoparticles by coupling SECCM with square-wave potentials using Pt nanoparticles as a model system. This system allows for high throughput probing of deposition conditions and evaluation of their effect on the final morphology and facet of nanoparticles. Electron microscopy and AFM confirmed tuning from rounded nanoparticles to nanocubes featuring Pt(100). The number of deposited nanoparticles from a few to decades can be controlled by the frequency, while the size of the nanoparticle can be controlled by the deposition time. This work serves as an initial step towards automated synthesis and characterization of single-facet metallic nanoparticles, offering significant potential for advancements in electrocatalysis and various other fields. While this work exploits potential control towards precision nanoparticle synthesis, exploring methods current control in the future could provide an additional layer of control over nanoparticle properties.



METHODS

Chemical and materials

Platinum solutions were prepared with sodium tetrachloride-platinate (II) hydrate (Sigma-Aldrich), sulfuric acid (98% Certified ACS Plus Grade, Fisher Chemical), and deionized water (18.2 M Ω cm, Synergy Water Purification System). A miniature silver/silver chloride reference electrode (ET072-1, eDAQ) was used as a quasi-reference counter electrode (QRCE) in SECCM, using a ME-series pipette holder (MEW-F10FL, Harvard Apparatus) to connect it to the micropipette.

Pipette preparation

Single channel nanopipettes of approximately 420 nm were fabricated from quartz glass capillaries (Q100-70-7.5, Sutter Instrument) using the P-2000 micropipette puller (Sutter Instrument). The pulling parameters were HEAT=490, FIL=1, VEL=30, DEL=145, PUL=200.

SECCM measurements

All SECCM experiments were conducted in a homebuilt scanning electrochemical probe system. This was controlled by an FPGA card (PCIe-7852R, National Instrument) through the Warwick Electrochemical Scanning Probe Microscopy Platform (WEC-SPM) software, kindly provided by the Warwick Electro-chemistry & Interfaces Group (WEIG). Two piezo systems were used to control movement; for the z-direction of the pipette a one-axis piezo-positioner (P-622.1CD, Physik Instrumente), and for the x-y plane movement of the substrate a two-axis piezo positioner (P-542.2CD, Physik Instrumente). This was all enclosed with a custom-built Faraday cage and mounted on a mechanical vibration isolator (BM-4, Minus K Technology). All current measurement was done with a Patch-clamp amplifier (Dagan Chem-clamp).

Square-wave voltammetry

A DAQ terminal block (NI BNC-2110 DAQ), manipulated through LabVIEW, was used as an arbitrary waveform generator. The output of the terminal block is controlled by the value of a triggering potential to be either a constant zero voltage DC potential or one of ten preprogrammed square-wave conditions. The output is summed to the DC potential (controlled by the FPGA card) using a summing amplifier sent to the Patch-clamp amplifier and applied to the substrate.



ASSOCIATED CONTENT

Supplementary Information

Experimental setup and procedure for square-wave voltammetry in SECCM, SEM of nanopipettes, additional voltammograms and electron micrographs for deposition under other square-wave conditions, and DC potential, RC constant calculation, and spatial distribution of nucleation sites.

ACKNOWLEDGEMENTS

The research is supported by the Welch Foundation (F-2158-2023040) and the Sloan Foundation (FG-2023-20317). We also acknowledge the use of the microscope facilities at the Texas Materials Institute at UT Austin. We are grateful to Dr. Xun Zhan for supporting the TEM analysis and Prof. Kim McKelvey for supporting the base software WEC-SPM.

REFERENCES

- (1) Anker, J. N.; Hall, W. P.; Lyandres, O.; Shah, N. C.; Zhao, J.; Van Duyne, R. P. Biosensing with Plasmonic Nanosensors. *Nat. Mater.* **2008**, *7* (6), 442–453. <https://doi.org/10.1038/nmat2162>.
- (2) Castañeda, A. D.; Brenes, N. J.; Kondajji, A.; Crooks, R. M. Detection of microRNA by Electrocatalytic Amplification: A General Approach for Single-Particle Biosensing. *J. Am. Chem. Soc.* **2017**, *139* (22), 7657–7664. <https://doi.org/10.1021/jacs.7b03648>.
- (3) Stark, W. J.; Stoessel, P. R.; Wohlleben, W.; Hafner, A. Industrial Applications of Nanoparticles. *Chem. Soc. Rev.* **2015**, *44* (16), 5793–5805. <https://doi.org/10.1039/C4CS00362D>.
- (4) Xie, S.; Choi, S.-I.; Xia, X.; Xia, Y. Catalysis on Faceted Noble-Metal Nanocrystals: Both Shape and Size Matter. *Curr. Opin. Chem. Eng.* **2013**, *2* (2), 142–150. <https://doi.org/10.1016/j.coche.2013.02.003>.
- (5) Tian, N.; Zhou, Z.-Y.; Sun, S.-G.; Ding, Y.; Wang, Z. L. Synthesis of Tetrahedral Platinum Nanocrystals with High-Index Facets and High Electro-Oxidation Activity. *Science* **2007**, *316* (5825), 732–735. <https://doi.org/10.1126/science.1140484>.



- (6) Xiao, C.; Lu, B.-A.; Xue, P.; Tian, N.; Zhou, Z.-Y.; Lin, X.; Lin, W.-F.; Sun, S.-G. High-Index-Facet- and High-Surface-Energy Nanocrystals of Metals and Metal Oxides as Highly Efficient Catalysts. *Joule* **2020**, *4* (12), 2562–2598. <https://doi.org/10.1016/j.joule.2020.10.002>.
- (7) Lim, J.; Liu, C.-Y.; Park, J.; Liu, Y.-H.; Senftle, T. P.; Lee, S. W.; Hatzell, M. C. Structure Sensitivity of Pd Facets for Enhanced Electrochemical Nitrate Reduction to Ammonia. *ACS Catal.* **2021**, *11* (12), 7568–7577. <https://doi.org/10.1021/acscatal.1c01413>.
- (8) Tang, J.-X.; Xiao, L.-P.; Xiao, C.; Tian, N.; Zhou, Z.-Y.; Sun, S.-G. Tetrahedral PdRh Nanocrystals with Tunable Composition as a Highly Efficient Electrocatalyst for Ethylene Glycol Oxidation. *J. Mater. Chem. A* **2021**, *9* (17), 11049–11055. <https://doi.org/10.1039/D1TA00663K>.
- (9) Ahmadi, T. S.; Wang, Z. L.; Green, T. C.; Henglein, A.; El-Sayed, M. A. Shape-Controlled Synthesis of Colloidal Platinum Nanoparticles. *Science* **1996**, *272* (5270), 1924–1925. <https://doi.org/10.1126/science.272.5270.1924>.
- (10) Zhang, L.; Xie, Z.; Gong, J. Shape-Controlled Synthesis of Au–Pd Bimetallic Nanocrystals for Catalytic Applications. *Chem. Soc. Rev.* **2016**, *45* (14), 3916–3934. <https://doi.org/10.1039/C5CS00958H>.
- (11) Liu, M.; Zheng, Y.; Zhang, L.; Guo, L.; Xia, Y. Transformation of Pd Nanocubes into Octahedra with Controlled Sizes by Maneuvering the Rates of Etching and Regrowth. *J. Am. Chem. Soc.* **2013**, *135* (32), 11752–11755. <https://doi.org/10.1021/ja406344j>.
- (12) Tian, N.; Zhou, Z.-Y.; Yu, N.-F.; Wang, L.-Y.; Sun, S.-G. Direct Electrodeposition of Tetrahedral Pd Nanocrystals with High-Index Facets and High Catalytic Activity for Ethanol Electrooxidation. *J. Am. Chem. Soc.* **2010**, *132* (22), 7580–7581. <https://doi.org/10.1021/ja102177r>.
- (13) Chen, L.-F.; Xie, A.-Y.; Lou, Y.-Y.; Tian, N.; Zhou, Z.-Y.; Sun, S.-G. Electrochemical Synthesis of Tetrahedral Cu Nanocrystals with High-Index Facets for Efficient Nitrate Electroreduction. *J. Electroanal. Chem.* **2022**, *907*, 116022. <https://doi.org/10.1016/j.jelechem.2022.116022>.
- (14) Glasscott, M. W.; Pendergast, A. D.; Goines, S.; Bishop, A. R.; Hoang, A. T.; Renault, C.; Dick, J. E. Electrosynthesis of High-Entropy Metallic Glass Nanoparticles for Designer, Multi-



- Functional Electrocatalysis. *Nat. Commun.* **2019**, *10* (1), 2650. <https://doi.org/10.1038/s41467-019-10303-z>.
- (15) Liu, J.; Fan, X.; Liu, X.; Song, Z.; Deng, Y.; Han, X.; Hu, W.; Zhong, C. Synthesis of Cubic-Shaped Pt Particles with (100) Preferential Orientation by a Quick, One-Step and Clean Electrochemical Method. *ACS Appl. Mater. Interfaces* **2017**, *9* (22), 18856–18864. <https://doi.org/10.1021/acsami.7b04267>.
- (16) Liu, Y.; Gokcen, D.; Bertocci, U.; Moffat, T. P. Self-Terminating Growth of Platinum Films by Electrochemical Deposition. *Science* **2012**, *338* (6112), 1327–1330. <https://doi.org/10.1126/science.1228925>.
- (17) Huang, K.; Clausmeyer, J.; Luo, L.; Jarvis, K.; Crooks, R. M. Shape-Controlled Electrodeposition of Single Pt Nanocrystals onto Carbon Nanoelectrodes. *Faraday Discuss.* **2018**, *210*, 267–280. <https://doi.org/10.1039/C8FD00018B>.
- (18) Xiao, C.; Tian, N.; Tang, J.-X.; Chen, L.-F.; Zhou, Z.-Y.; Sun, S.-G. Electrolyte Effects on the Shape-Controlled Synthesis of Pt Nanocrystals by Electrochemical Square-Wave Potential Method. *J. Electroanal. Chem.* **2023**, *935*, 117344. <https://doi.org/10.1016/j.jelechem.2023.117344>.
- (19) Liu, X.; Wang, K.; Zhou, L.; Pu, H.; Zhang, T.; Jia, J.; Deng, Y. Shape-Controlled Synthesis of Concave Pt and Willow-Like Pt Nanocatalysts via Electrodeposition with Hydrogen Adsorption/Desorption and Investigation of Their Electrocatalytic Performances toward Ethanol Oxidation Reaction. *ACS Sustain. Chem. Eng.* **2020**, *8* (16), 6449–6457. <https://doi.org/10.1021/acssuschemeng.0c00967>.
- (20) Ebejer, N.; Güell, A. G.; Lai, S. C. S.; McKelvey, K.; Snowden, M. E.; Unwin, P. R. Scanning Electrochemical Cell Microscopy: A Versatile Technique for Nanoscale Electrochemistry and Functional Imaging. *Annu. Rev. Anal. Chem.* **2013**, *6* (1), 329–351. <https://doi.org/10.1146/annurev-anchem-062012-092650>.
- (21) Gaudin, L. F.; Wright, I. R.; Harris-Lee, T. R.; Jayamaha, G.; Kang, M.; Bentley, C. L. Five Years of Scanning Electrochemical Cell Microscopy (SECCM): New Insights and Innovations. *Nanoscale* **2024**, *16* (26), 12345–12367. <https://doi.org/10.1039/D4NR00859F>.
- (22) Xu, X.; Valavanis, D.; Ciocci, P.; Confederat, S.; Marcuccio, F.; Lemineur, J.-F.; Actis, P.; Kanoufi, F.; Unwin, P. R. The New Era of High-Throughput Nanoelectrochemistry. *Anal. Chem.* **2023**, *95* (1), 319–356. <https://doi.org/10.1021/acs.analchem.2c05105>.



- (23) Li, M.; Ye, K.-H.; Qiu, W.; Wang, Y.; Ren, H. Heterogeneity between and within Single Hematite Nanorods as Electrocatalysts for Oxygen Evolution Reaction. *J. Am. Chem. Soc.* **2022**, *144* (12), 5247–5252. <https://doi.org/10.1021/jacs.2c00506>.
- (24) Zhao, J.; Wang, M.; Peng, Y.; Ni, J.; Hu, S.; Zeng, J.; Chen, Q. Exploring the Strain Effect in Single Particle Electrochemistry Using Pd Nanocrystals. *Angew. Chem. Int. Ed.* **2023**, *62* (30), e202304424. <https://doi.org/10.1002/anie.202304424>.
- (25) Rahman, Md. M.; Tolbert, C. L.; Saha, P.; Halpern, J. M.; Hill, C. M. On-Demand Electrochemical Fabrication of Ordered Nanoparticle Arrays Using Scanning Electrochemical Cell Microscopy. *ACS Nano* **2022**, *16* (12), 21275–21282. <https://doi.org/10.1021/acsnano.2c09336>.
- (26) Ciocci, P.; Valavanis, D.; Meloni, G. N.; Lemineur, J.; Unwin, P. R.; Kanoufi, F. Optical Super-Localisation of Single Nanoparticle Nucleation and Growth in Nanodroplets. *ChemElectroChem* **2023**, *10* (9), e202201162. <https://doi.org/10.1002/celec.202201162>.
- (27) Lee, H.; Matthews, K. C.; Zhan, X.; Warner, J. H.; Ren, H. Precision Synthesis of Bimetallic Nanoparticles via Nanofluidics in Nanopipets. *ACS Nano* **2023**, *17* (22), 22499–22507. <https://doi.org/10.1021/acsnano.3c06011>.
- (28) Mondaca-Medina, E.; García-Carrillo, R.; Lee, H.; Wang, Y.; Zhang, H.; Ren, H. Nanoelectrochemistry in Electrochemical Phase Transition Reactions. *Chem. Sci.* **2023**, *14* (28), 7611–7619. <https://doi.org/10.1039/D3SC01857A>.
- (29) Marković, N. M.; Grgur, B. N.; Ross, P. N. Temperature-Dependent Hydrogen Electrochemistry on Platinum Low-Index Single-Crystal Surfaces in Acid Solutions. *J. Phys. Chem. B* **1997**, *101* (27), 5405–5413. <https://doi.org/10.1021/jp970930d>.
- (30) Lapp, A. S.; Duan, Z.; Henkelman, G.; Crooks, R. M. Combined Experimental and Theoretical Study of the Structure of AuPt Nanoparticles Prepared by Galvanic Exchange. *Langmuir* **2019**, *35* (50), 16496–16507. <https://doi.org/10.1021/acs.langmuir.9b03192>.
- (31) Martínez-Rodríguez, R. A.; Vidal-Iglesias, F. J.; Solla-Gullón, J.; Cabrera, C. R.; Feliu, J. M. Synthesis and Electrocatalytic Properties of H₂ SO₄ -Induced (100) Pt Nanoparticles Prepared in Water-in-Oil Microemulsion. *ChemPhysChem* **2014**, *15* (10), 1997–2001. <https://doi.org/10.1002/cphc.201400056>.



The data supporting this article have been included as the main figures or as part of the Supplementary Information.

Open Access Article. Published on 23 janvier 2025. Downloaded on 2025-01-25 00:32:02.
This article is licensed under a Creative Commons Attribution-NonCommercial 3.0 Unported Licence.

